

PM/99-08
June 1999

Precision Tests in e^+e^- and $\gamma\gamma$ processes and Virtual New Physics Effects ¹

F.M. Renard

Physique Mathématique et Théorique, UMR-CNRS 5825
Université Montpellier II, F-34095 Montpellier Cedex 5.

**Summary of works done in collaboration with
M. Beccaria, P. Ciafaloni, D. Comelli, G.J. Gounaris, J. Layssac,
P. Porfyriadis, S. Spagnolo, C. Verzegnassi.**

Abstract

We report on several works dealing with precision tests of the Standard Model (SM) and beyond, in the processes $e^+e^- \rightarrow f\bar{f}$ ($f = \text{lepton or quarks}$) and $\gamma\gamma \rightarrow \gamma\gamma, \gamma Z$. We first point out a set of remarkable properties of the SM amplitudes and observables at high energies, at tree level and at 1-loop, like "Sudakov" behaviour or the dominance of purely imaginary non-flip amplitudes due to the WWWW box. We then consider various types of virtual NP contributions due to supersymmetry, anomalous gauge boson couplings, technicolour and extended gauge structures. Effects at LEP2 and LC (in particular with a laser backscattering $\gamma\gamma$ mode) are discussed. We point out specific features like clear threshold enhancements.

¹Contribution to LP99, International Symposium on Lepton-Photon Interactions, Stanford, Aug. 1999.

In this contribution we report on several works [1, 2, 3, 4, 5] dealing with the search for physics beyond the Standard Model (SM) that could appear through virtual effects in processes measurable at present and future e^+e^- colliders. We successively consider (A) 4-fermion processes $e^+e^- \rightarrow f\bar{f}$ ($f = \text{lepton or quarks}$) and (B) photon-photon collisions $\gamma\gamma \rightarrow \gamma\gamma, \gamma Z$. In both cases we look for virtual new physics (NP) effects arising at 1-loop. This should be especially interesting when no direct production of the NP degrees of freedom is allowed or detectable or well identifiable. Each class of processes have specific features which allow to reach these 1-loop NP effects. In (A) it is the very high accuracy of the experiments; first at Z peak, where it allows to establish the SM properties at a very high accuracy; then, at a high luminosity and a high energy linear collider (LC), where departures from SM should be enhanced. In (B) it is the fact that SM contributions only starts at 1-loop, at the same order as the NP contributions.

(A) Virtual NP effects in $e^-e^- \rightarrow f\bar{f}$ processes

As we just mentioned, the basic ingredient is the measurement of SM parameters at a very high accuracy at Z peak and at low energy. In order to exploit this fact in an automatic way and to look for departures due to NP at higher energies, it is convenient to use the so-called "Z-peak subtracted representation" [6]. It consists in using as inputs $\alpha(0)$, M_Z and the Z partial widths and asymmetries measured at Z peak. At higher energies the amplitudes and the usual observables are then expressed in terms of sets of four functions called $\tilde{\Delta}_{\alpha,ef}(q^2, \theta)$, $R_{ef}(q^2, \theta)$, $V_{ef}^{\gamma Z}(q^2, \theta)$, $V_{ef}^{Z\gamma}(q^2, \theta)$. These functions are directly associated to subtracted forms ($F_i(q^2) - F_i(M_Z^2)$) of the $\gamma\gamma$, ZZ , γZ , $Z\gamma$ Lorentz structures of the e^+e^- annihilation process on which the 1-loop SM or NP contributions are projected [6]. Owing to their subtracted form, the SM or NP contributions to these functions are automatically finite and their effects in the various observables (cross sections σ_f , forward-backward asymmetries $A_{FB,f} = \sigma_f^{FB}/\sigma_f$ and polarized asymmetries $A_{LR,f} = \sigma_{LR,f}/\sigma_f$ $A_{FB,f}^{pol} = \sigma_{LR,f}^{FB}/\sigma_f$) are easily computed through Born-like expressions. The explicit expressions of the observables are given in Appendix A. They allow a very fast computation of any SM or NP effect, analytically or numerically.

— A first application: the 1-loop pure SM case contributions.

We have collected the full set of 1-loop electroweak SM contributions to $e^+e^- \rightarrow f\bar{f}$ and their explicit contributions to the four functions in [7]. A computer code (PALM) has been constructed which also includes the ISR effects. We have checked that this program which runs in a very fast way, reproduces at a very good accuracy the results previously obtained by existing codes based on conventional representations. The advantage of our representation is to allow to trace back in a very simple and clear way each contribution to the various observables. We have then looked at the high energy behaviour of these 1-loop contributions. Keeping only their $\ln s$ and the $\ln^2 s$ terms we have established extremely simple expressions for these four functions and for the corrections to the various observables [1]. For example the cross section $\sigma(e^+e^- \rightarrow \mu^+\mu^-)$ becomes:

$$\begin{aligned}
\sigma_\mu = & \sigma_\mu^B \left[1 + \frac{\alpha(M_Z^2)}{4\pi} \left\{ (7.72N - 20.58) \ln \frac{q^2}{M_Z^2} + 35.27 \ln \frac{q^2}{M_W^2} - 4.59 \ln^2 \frac{q^2}{M_W^2} \right. \right. \\
& \left. \left. + 4.79 \ln \frac{q^2}{M_Z^2} - 1.43 \ln^2 \frac{q^2}{M_Z^2} \right\} + \dots \right] \tag{1}
\end{aligned}$$

where $\sigma_\mu^{(B)} = 0.11106/q^2(fb/TeV^2)$. The first $\ln \frac{q^2}{M_Z^2}$ term corresponds to the Renormalization Group (RG) contribution (self-energy diagrams and universal Bosonic triangles; $N = 3$ is the number of fermionic generations), whereas the other (linear and quadratic) logarithmic terms are of "Sudakov" type. The \ln^2 s terms come from well identified specific triangle diagrams with one gauge boson exchanged and from box diagrams with a pair of gauge bosons. Similar expressions for the other muonic or hadronic observables can be found in [1].

As one can see in Fig.1, the RG linear logarithmic contribution is smaller than the Sudakov one. Although the linear and quadratic Sudakov contributions have opposite signs, the total effect is much different from the RG one, so that ignoring them would give a completely wrong result. One also sees that in the multi-TeV range the individual contributions reach a relative magnitude of the 10% level thus raising the question of possible non negligible 2-loop effects.

The dots that appear in the brackets of eqs.(1) refer to the "non-leading" terms. These could either be constants or $O(\frac{1}{q^2})$ components whose asymptotic effect vanishes. We have checked that indeed, in the TeV region, these asymptotic results agree at the permille level with exact SM predictions obtained from the semianalytic program (PALM)[7] and from TOPAZ0 [8]. At non asymptotic energies, for example in the range $0.2 TeV < \sqrt{s} < 1 TeV$, one can globally replace the dots by fitted constants. In the case of σ_μ the dots can be replaced by $-13.5 \frac{\alpha(M_Z^2)}{\pi}$, which optimizes the approximation at $0.5 TeV$.

Eq.(1) and similar ones obtained in ref.[1] provide very good descriptions of the various polarized and unpolarized observables in $e^+e^- \rightarrow f\bar{f}$ at high energy. They can be useful when discussing the potential of future colliders for testing the Standard Model predictions and for looking at departures due to NP contributions.

— Supersymmetric effects.

The second application concerns Supersymmetry effects. We have added to SM diagrams the corresponding sets of self-energy, vertex and box diagrams with supersymmetric partners, sfermions and gauginos. The results now depend on the supersymmetric model and the corresponding parameters which are used. We have considered the MSSM [9] (whose parameters are $M_1, M_2, \mu, \tan\beta$) with the GUT relation between the $SU(2) \otimes U(1)$ gauginos soft mass parameters $M_1 = \frac{5}{3} \tan^2 \theta_w M_2$. We have first looked at the possibility of a signal in $e^+e^- \rightarrow f\bar{f}$ at LEP2 due to a light chargino [2].

For illustration we fix the light chargino mass at 105 GeV, the sleptons physical masses at 120 GeV and the squarks physical ones at 200 GeV. We set $\tan \beta = 1.6$, and verified

that varying it from 1.6 to 40 does not produce any appreciable change. With this choice, we computed the relative SUSY shifts on the three chosen observables \mathcal{O}_i , $\Delta^{\text{SUSY}}\mathcal{O} \equiv \frac{\mathcal{O}^{\text{SUSY}} - \mathcal{O}^{\text{SM}}}{\mathcal{O}^{\text{SM}}}$ ($\mathcal{O}_{1,2,3} = \sigma_\mu, \sigma_5, A_{FB,\mu}$).

Fig. (2) shows the variations of the relative effects on the observables when $\sqrt{q^2} = 200$ GeV and μ varies in its allowed range. One sees that the size of the SUSY contribution to the muon asymmetry remains systematically negligible, well below the six-seven permille limit that represents an optimistic experimental reach in this case [11]. On the contrary, in the case of the muon and hadronic cross sections, the size of the effect approaches, for large $|\mu|$ values, a limit of six permille in σ_μ and four permille in σ_5 that represent a conceivable experimental reach, at the end of the overall LEP2 running period.

This explains in fact our choice of the value $M_{\chi_{light}^+} = 105$ GeV with LEP2 limit at 200 GeV; other couples of the light chargino mass and of the LEP2 limit separated by a larger gap would produce a smaller effect, i.e. an unobservable one. On the other hand, smaller gaps (e.g. a lighter but still unproduced chargino or a larger LEP2 limit) would increase the effect, towards the one percent values that appear to be experimentally realistic.

We have analyzed various possibilities, $|\mu| \gg M_2$ (“gaugino like”), $M_2 \gg |\mu|$ (“higgsino like”). We present in Fig. (3) the energy behaviour of the three main unpolarized observables in the high $|\mu|$ case, showing a remarkable threshold enhancement.

We have also considered the different situation, where the lightest chargino is “heavy” and decoupled, setting its mass equal to 300 GeV, and assuming that all sleptons are now “light” (i.e. $m_{\tilde{l}} = 105$ GeV). The signal has almost completely disappeared. This is the consequence of the P-wave depression factor $\approx q^2 - 4m_{\tilde{l}}^2$ which appears for spinless sfermions and which washes out the threshold enhancement [2].

Applications to a 500 GeV LC are in progress.

— Residual NP effects.

We have considered NP effects leading to anomalous gauge boson couplings. This type of effects is usually described by a set of $SU(2) \times U(1)$ gauge invariant operators. We have chosen the linear representation and the set of $dim = 6$ operators [10]. Among them a subset dubbed “blind” is constrained by direct measurements in $e^+e^- \rightarrow W^+W^-$ and another set dubbed “superblind” by $e^+e^- \rightarrow HZ, H\gamma$ [11]. The remaining “non-blind” set of 4 operators $\mathcal{O}_{DW}, \mathcal{O}_{DB}, \mathcal{O}_{BW}, \mathcal{O}_{\Phi 1}$ is responsible for modifications of the gauge boson propagators:

$$\mathcal{L}^{(NB)} = \frac{f_{DW}}{\Lambda^2}\mathcal{O}_{DW} + \frac{f_{DB}}{\Lambda^2}\mathcal{O}_{DB} + \frac{f_{BW}}{\Lambda^2}\mathcal{O}_{BW} + \frac{f_{\Phi,1}}{\Lambda^2}\mathcal{O}_{\Phi,1} \quad (2)$$

$$\mathcal{O}_{DW} = Tr([D_\mu, \vec{W}_{\nu\rho}][D^\mu, \vec{W}^{\nu\rho}]) \quad , \quad (3)$$

$$\mathcal{O}_{DB} = -\frac{g^2}{2}(\partial_\mu B_{\nu\rho})(\partial^\mu B^{\nu\rho}) \quad , \quad (4)$$

$$\mathcal{O}_{BW} = \Phi^\dagger B_{\mu\nu} \vec{\tau} \cdot \vec{W}^{\mu\nu} \Phi \quad , \quad (5)$$

$$\mathcal{O}_{\Phi_1} = (D_\mu \Phi^\dagger \Phi)(\Phi^\dagger D^\mu \Phi) \quad , \quad (6)$$

They have already been constrained by measurements of $e^+e^- \rightarrow f\bar{f}$ at Z peak [10], but it has been shown that improvements can be expected by measurements of $e^+e^- \rightarrow f\bar{f}$ cross sections at higher energies[12, 13]. Using the virtues of the Z peak subtracted representation, we have shown that the largest improvements expected from LEP2 or LC measurements will occur for the operators \mathcal{O}_{DW} , \mathcal{O}_{DB} which lead to strong energy dependent effects. In a new analysis [14] including low energy and Z peak data together with expectations at LEP2 we have obtained the results shown in Fig.4, which for example amount to improve the limits as follows:

	δf_{DW}	δf_{BW}	δf_{DB}	$\delta f_{\Phi,1}$
Low	0.28	1.43	6.27	0.088
Low+High	0.18	0.32	1.15	0.035

Table1: Bounds on the anomalous gauge couplings obtained with a combined fit of present and future experimental data. The definition of the parameter uncertainties adopted here is the 1σ error in the χ^2 minimization. **Low** refers to the results from LEP1, APV and from the measurement of M_W , **High** to the cross-section and asymmetry measurements at LEP2.

At a 500 GeV linear collider, with a luminosity of $50 fb^{-1}$ the sensitivity is expected to improve at the level of $\delta f_{DW} = 0.06$, $\delta f_{BW} = 0.27$, $\delta f_{DB} = 0.22$, $\delta f_{\Phi,1} = 0.04$ in [13] and $\delta f_{DW} = 0.025$, $\delta f_{DB} = 0.16$ with unpolarized beams, and $\delta f_{DW} = 0.014$, $\delta f_{DB} = 0.08$ with polarized beams in [15]. With a higher LC luminosity [16], these numbers should scale like $\mathcal{L}_{ee}^{-\frac{1}{2}}$.

— Other types of NP.

We close this subsection by mentioning that the "Z-peak subtracted representation" has also been used for establishing constraints on the effects of Higher Vector Bosons, either of gauge nature (for example Z') or of composite nature (for example Technicolour resonances). See ref.[6, 17] where limits for masses and couplings were given.

(B) Virtual NP effects in $\gamma\gamma \rightarrow \gamma\gamma$, γZ , ZZ processes

These processes are particularly interesting because the SM contribution only starts at 1-loop[18]; a contrario $\gamma\gamma \rightarrow W^+W^-$ has tree level contributions. Therefore these neutral processes provide a clean window to new physics. The laserbackscattering device should allow to provide intense and high energy photon beams at an e^+e^- linear collider.

For example the TESLA project [16] announce the possibility of accumulating an e^+e^- luminosity of about $1000 fb^{-1}$ in two or three years. The photon fluxes $dL_{\gamma\gamma}/d\tau$ that multiply the e^+e^- luminosity are expected to be of the order of 1 or even more for the range $E_{cm}^{\gamma\gamma} \lesssim 0.8 E_{cm}^{ee}$ [19]. This should allow to make precise measurements of these processes whose cross sections are of the order of a few tens of fb . NP effects leading to departures from SM at the level of 1 percent should then be observable.

A special feature of the SM amplitudes in the above processes is the dominance of a few purely imaginary non flip amplitudes [3]; for example in $\gamma\gamma \rightarrow \gamma\gamma$:

$$F_{\pm\pm\pm\pm}(\hat{s}, \hat{t}, \hat{u}) \simeq -i 16\pi\alpha^2 \left[\frac{\hat{s}}{\hat{u}} \text{Ln} \left| \frac{\hat{u}}{M_W^2} \right| + \frac{\hat{s}}{\hat{t}} \text{Ln} \left| \frac{\hat{t}}{M_W^2} \right| \right], \quad (7)$$

$$F_{\pm\mp\pm\mp}(\hat{s}, \hat{t}, \hat{u}) \simeq -i 12\pi\alpha^2 \frac{\hat{s} - \hat{t}}{\hat{u}} + i \frac{8\pi\alpha^2}{\hat{u}^2} (4\hat{u}^2 - 3\hat{s}\hat{t}) \left[\text{Ln} \left| \frac{\hat{t}}{\hat{s}} \right| \right] \\ -i 16\pi\alpha^2 \left[\frac{\hat{u}}{\hat{s}} \text{Ln} \left| \frac{\hat{u}}{M_W^2} \right| + \frac{\hat{u}^2}{\hat{s}\hat{t}} \text{Ln} \left| \frac{\hat{t}}{M_W^2} \right| \right], \quad (8)$$

Similar amplitudes appear in $\gamma\gamma \rightarrow \gamma Z$ with a coupling factor c_W/s_W and M_Z^2/s corrections [5]. In the high energy limit, the dominant 1-loop SM contributions satisfy the relations

$$F_{\gamma\gamma \rightarrow \gamma Z}^W \simeq \frac{c_W}{s_W} F_{\gamma\gamma \rightarrow \gamma\gamma}^W \quad (9)$$

$$F_{\gamma\gamma \rightarrow \gamma Z}^f \simeq \frac{g_{Vf}^Z}{Q_f} F_{\gamma\gamma \rightarrow \gamma\gamma}^f \quad (10)$$

with, for a standard fermion f ,

$$g_{Vf}^Z = \frac{t_3^f - 2Q_f s_W^2}{2c_W s_W} \quad (11)$$

The dominance of imaginary parts is due to the large W box contribution. This is confirmed by an exact numerical computation of all SM amplitudes as we can see in Fig.5. This situation is reminiscent of the Pomeron dominance in VDM processes at the hadronic GeV scale.

Non standard effects due to the interference with SM will therefore appear predominantly when the amplitudes have large imaginary parts. Typical examples are threshold enhancements, resonances, unitarity saturating phenomena [3, 20, 21]. A few illustrations are reproduced in Fig.6. On the opposite, note that residual NP effects described by effective lagrangians giving real amplitudes, are not favored.

Beam polarization should allow to make checks of the nature of the NP effects. Assuming 80 % electron beam polarization and fully polarized laser beams, polarized photon-photon fluxes are expected to be large [22, 4]. They allow to consider 8 different types of quantities in $\gamma\gamma \rightarrow \gamma Z$ (they reduce to 6 in $\gamma\gamma \rightarrow \gamma\gamma$) denoted $\bar{\sigma}_{ij}$ and listed in Appendix B (see also [4] and in [5]).

We have developed the study of supersymmetric effects, considering contributions from fermionic and scalar partners. In Fig 7-10, we have illustrated the $\gamma\gamma \rightarrow \gamma\gamma$, Z cases with one gaugino and one slepton. As the corresponding (gaugino, slepton) box amplitudes in $\gamma\gamma \rightarrow \gamma\gamma$ depend on the coupling factor Q^4 , the result equally apply to any other (fermion, scalar) with the same mass. So this process provides model independent tests. In addition it is experimentally clean. As opposed to real production of new particles this search for virtual effects is not affected by the complexity of the decay modes.

The $\gamma\gamma \rightarrow \gamma Z$ process is also clean; all Z modes (triggerred by the associated photon) can be used. The rate is about 6 times larger than the $\gamma\gamma \rightarrow \gamma\gamma$ one. The couplings factor in the box due a particle X is now $Q_X^3 g_{VX}^Z$. Its presence should allow, first to confirm a possible effect in $\gamma\gamma \rightarrow \gamma\gamma$, secondly to disentangle different possibilities [23] which differ by the magnitude like chargino/higgsino, or even the sign of g_{VX}^Z like slepton-L/slepton-R, and lead, through the interference term, to corresponding departures from SM predictions.

Similar applications can be done to other types of virtual contributions, for example new fermions and bosons in Technicolour schemes [20].

The process $\gamma\gamma \rightarrow ZZ$ should give further informations (in particular on the Higgs sector) and its study is in progress.

Conclusions

We have pointed out several remarkable properties of the processes $e^+e^- \rightarrow f\bar{f}$ and $\gamma\gamma \rightarrow \gamma\gamma$, γZ at high energies and their implications for the search of virtual NP effects. This search requires the availability of high energy and high luminosity e^+e^- and $\gamma\gamma$ colliders.

There are historical examples about the way precision tests can give hints about new particles and interactions. Recently, at Z peak, we had several examples with neutrino counting, the excellent hint for the top quark and maybe now a hint for a light Higgs boson.

At higher energies the search for NP in standard processes may proceed in a similar way, in the sense that hints may come from precision measurements revealing the presence of some anomalous contribution. The high accuracy at which the SM parameters have been measured at Z peak and at low energies, put together with accurate measurements at high energies should be the clue to this type of searches.

The "Z-peak subtracted representation", that we have emphasized in this report, is especially suitable for the studies in $e^+e^- \rightarrow f\bar{f}$ at high energies, as it takes into account in an automatic way, the measurements at Z peak and as it singles out the departures due to new contributions rising with the energy. We have treated several examples taken from NP predicted by Supersymmetry or Technicolour models.

In $\gamma\gamma \rightarrow \gamma\gamma$, γZ processes the situation is somewhat different because the SM contribution and the NP contribution both start at 1-loop. This privileged situation of NP effects may compensate the weakness of the corresponding cross sections.

For example we have shown, both in e^+e^- and in $\gamma\gamma$ collisions that NP signals may come in standard processes from visible "threshold enhancements". This method is independent of the one which consists in looking at the direct production of new particles and

studying their decay modes. It should be especially advantageous for the search of new particles decaying through a long chain of processes, which are difficult to extract from a background (ex. gauginos, sleptons or PGB's).

Another remark is that in $\gamma\gamma \rightarrow \gamma\gamma$ the unpolarized cross section (because of the Q^4 box contribution) cumulates positive contributions from NP above threshold. Thus, in the high energy limit, this cross section provides a kind of counting of the number of states involved in the loop. For example, if SUSY is realized in Nature below the TeV-scale, then it would be quite plausible that a chargino, as well as all six charged sleptons and the \tilde{t}_1 squark, lie in a limited mass range. In such a case, a clear signal could be observable.

The process $\gamma\gamma \rightarrow \gamma Z$ with a larger cross section and the presence of the Z coupling as well as the availability of polarized $\gamma\gamma$ collisions should give additional informations about the nature of the particles produced.

We therefore conclude, that important physical information could arise from the study of the $e^+e^- \rightarrow f\bar{f}$ and the $\gamma\gamma \rightarrow \gamma\gamma, \gamma Z$ processes, and that this certainly constitutes an argument favoring the availability of a high energy, high luminosity Linear Collider and its laser $\gamma\gamma$ option.

Appendix A: Expressions of $e^+e^- \rightarrow f\bar{f}$ observables in the Z -peak subtracted representation.

The unpolarized cross section for $e^+e^- \rightarrow f\bar{f}$

$$\sigma_f = \frac{4\pi N_f q^2}{3} \int_{-1}^{+1} d\cos\theta \left[\frac{3}{8}(1 + \cos^2\theta)U_{11} + \frac{3}{4}\cos\theta U_{12} \right] \quad (12)$$

and the forward-backward asymmetry

$$\sigma_f^{FB} = \frac{4\pi N_f q^2}{3} \left\{ \int_0^{+1} - \int_{-1}^0 \right\} d\cos\theta \left[\frac{3}{8}(1 + \cos^2\theta)U_{11} + \frac{3}{4}\cos\theta U_{12} \right] \quad (13)$$

$$A_{FB,f} = \sigma_f^{FB} / \sigma_f \quad (14)$$

are expressed in terms of U_{11} and U_{12} :

$$\begin{aligned} U_{11} = & \frac{\alpha^2(0)Q_f^2}{q^4} [1 + 2\delta\tilde{\Delta}^{(lf)}\alpha(q^2)] \\ & + 2[\alpha(0)|Q_f|] \frac{q^2 - M_Z^2}{q^2((q^2 - M_Z^2)^2 + M_Z^2\Gamma_Z^2)} \left[\frac{3\Gamma_l}{M_Z} \right]^{1/2} \left[\frac{3\Gamma_f}{N_b M_Z} \right]^{1/2} \frac{\tilde{v}_l \tilde{v}_f}{(1 + \tilde{v}_l^2)^{1/2} (1 + \tilde{v}_f^2)^{1/2}} \\ & \times [1 + \tilde{\Delta}^{(lf)}\alpha(q^2) - R^{(lf)}(q^2) - 4s_{lc_l} \left\{ \frac{1}{\tilde{v}_l} V_{\gamma Z}^{(lf)}(q^2) + \frac{|Q_f|}{\tilde{v}_f} V_{Z\gamma}^{(lf)}(q^2) \right\}] \\ & + \frac{\left[\frac{3\Gamma_l}{M_Z} \right] \left[\frac{3\Gamma_f}{N_f M_Z} \right]}{(q^2 - M_Z^2)^2 + M_Z^2\Gamma_Z^2} \\ & \times [1 - 2R^{(lf)}(q^2) - 8s_{lc_l} \left\{ \frac{\tilde{v}_l}{1 + \tilde{v}_l^2} V_{\gamma Z}^{(lf)}(q^2) + \frac{\tilde{v}_f |Q_f|}{(1 + \tilde{v}_f^2)} V_{Z\gamma}^{(lf)}(q^2) \right\}] , \end{aligned} \quad (15)$$

$$\begin{aligned} U_{12} = & 2[\alpha(0)|Q_f|] \frac{q^2 - M_Z^2}{q^2((q^2 - M_Z^2)^2 + M_Z^2\Gamma_Z^2)} \left[\frac{3\Gamma_l}{M_Z} \right]^{1/2} \left[\frac{3\Gamma_f}{N_f M_Z} \right]^{1/2} \frac{1}{(1 + \tilde{v}_l^2)^{1/2} (1 + \tilde{v}_f^2)^{1/2}} \\ & \times [1 + \tilde{\Delta}^{(lf)}\alpha(q^2) - R^{(lf)}(q^2)] \\ & + \frac{\left[\frac{3\Gamma_l}{M_Z} \right] \left[\frac{3\Gamma_f}{N_f M_Z} \right]}{(q^2 - M_Z^2)^2 + M_Z^2\Gamma_Z^2} \left[\frac{4\tilde{v}_l \tilde{v}_f}{(1 + \tilde{v}_l^2)(1 + \tilde{v}_f^2)} \right] \\ & \times [1 - 2R^{(lf)}(q^2) - 4s_{lc_l} \left\{ \frac{1}{\tilde{v}_l} V_{\gamma Z}^{(lf)}(q^2) + \frac{|Q_f|}{\tilde{v}_f} V_{Z\gamma}^{(lf)}(q^2) \right\}] , \end{aligned} \quad (16)$$

$$(17)$$

In the left-right polarized case, we have the two other combinations U_{21} and U_{22} :

$$\sigma_{LR,f} = \frac{4\pi N_f q^2}{3} \int d\cos\theta \left[\frac{3}{8}(1 + \cos^2\theta)U_{21} + \frac{3}{4}\cos\theta U_{22} \right] \quad (18)$$

$$\sigma_{LR,f}^{FB} = \frac{4\pi N_f q^2}{3} \left\{ \int_0^{+1} - \int_{-1}^0 \right\} d\cos\theta \left[\frac{3}{8}(1 + \cos^2\theta)U_{21} + \frac{3}{4}\cos\theta U_{22} \right] \quad (19)$$

$$A_{LR,f} = \sigma_{LR,f}/\sigma_f \quad A_{FB,f}^{pol} = \sigma_{LR,f}^{FB}/\sigma_f \quad (20)$$

$$\begin{aligned} U_{21} = & 2[\alpha(0)|Q_f|] \frac{q^2 - M_Z^2}{q^2((q^2 - M_Z^2)^2 + M_Z^2\Gamma_Z^2)} \left[\frac{3\Gamma_l}{M_Z} \right]^{1/2} \left[\frac{3\Gamma_f}{N_f M_Z} \right]^{1/2} \frac{\tilde{v}_f}{(1 + \tilde{v}_l^2)^{1/2}(1 + \tilde{v}_f^2)^{1/2}} \\ & \times [1 + \tilde{\Delta}^{(lf)}\alpha(q^2) - R^{(lf)}(q^2) - \frac{4s_l c_l |Q_f|}{\tilde{v}_f} V_{Z\gamma}^{(lf)}(q^2)] + \frac{\left[\frac{3\Gamma_l}{M_Z} \right] \left[\frac{3\Gamma_f}{N_f M_Z} \right]}{(q^2 - M_Z^2)^2 + M_Z^2\Gamma_Z^2} \left[\frac{2\tilde{v}_l}{(1 + \tilde{v}_l^2)} \right] \\ & \times [1 - 2R^{(lf)}(q^2) - 4s_l c_l \left\{ \frac{1}{\tilde{v}_l} V_{\gamma Z}^{(lf)}(q^2) + \frac{2\tilde{v}_f |Q_f|}{(1 + \tilde{v}_f^2)} V_{Z\gamma}^{(lf)}(q^2) \right\}] , \end{aligned} \quad (21)$$

$$\begin{aligned} U_{22} = & 2[\alpha(0)|Q_f|] \frac{q^2 - M_Z^2}{q^2((q^2 - M_Z^2)^2 + M_Z^2\Gamma_Z^2)} \left[\frac{3\Gamma_l}{M_Z} \right]^{1/2} \left[\frac{3\Gamma_f}{N_f M_Z} \right]^{1/2} \frac{\tilde{v}_l}{(1 + \tilde{v}_l^2)^{1/2}(1 + \tilde{v}_f^2)^{1/2}} \\ & \times [1 + \tilde{\Delta}^{(lf)}\alpha(q^2) - R^{(lf)}(q^2) - \frac{4s_l c_l}{\tilde{v}_l} V_{\gamma Z}^{(lf)}(q^2)] + \frac{\left[\frac{3\Gamma_l}{M_Z} \right] \left[\frac{3\Gamma_f}{N_f M_Z} \right]}{(q^2 - M_Z^2)^2 + M_Z^2\Gamma_Z^2} \left[\frac{2\tilde{v}_f}{(1 + \tilde{v}_f^2)} \right] \\ & \times [1 - 2R^{(lf)}(q^2) - 4s_l c_l \left\{ \frac{2\tilde{v}_l}{(1 + \tilde{v}_l^2)} V_{\gamma Z}^{(lf)}(q^2) + \frac{|Q_f|}{\tilde{v}_f} V_{Z\gamma}^{(lf)}(q^2) \right\}] . \end{aligned} \quad (22)$$

N_f is the conventional color factor which contains standard QCD corrections, the inputs are $\alpha(0)$, M_Z and Γ_l , Γ_f , $\tilde{v}_e \equiv 1 - 4s_l^2$, $\tilde{v}_f \equiv 1 - 4|Q_f|s_f^2$ measured at Z peak.

This applies to $e^+e^- \rightarrow leptons$ ($f=1$) and to $e^+e^- \rightarrow hadrons$ (summing $\sum_f \sigma_f$ and $\sum_f \sigma_{LR,f}$ over $f = 2u + 2d + b$).

Each application then consists in considering contributions to the four functions $\tilde{\Delta}^{(lf)}\alpha(q^2)$, $R^{(lf)}(q^2)$, $V_{\gamma Z}^{(lf)}(q^2)$ and $V_{Z\gamma}^{(lf)}(q^2)$. These are obtained by projecting the considered SM or NP amplitude on the $\gamma\gamma$, ZZ , γZ and $Z\gamma$ Born Lorentz structures [6].

For example in the case of universal modifications to the gauge boson propagators due to the $dim = 6$ operators \mathcal{O}_{DW} , \mathcal{O}_{DB} one gets [14]:

$$\tilde{\Delta}_\alpha^{(AGC)}(q^2) = -8\pi\alpha \frac{q^2}{\Lambda^2} [f_{DW} + f_{DB}] \quad (23)$$

$$R^{(AGC)}(q^2) = 8\pi\alpha \frac{(q^2 - M_Z^2)}{\Lambda^2} \left[\frac{c_l^2}{s_l^2} f_{DW} + \frac{s_l^2}{c_l^2} f_{DB} \right] \quad (24)$$

$$V^{(AGC)}(q^2) = 8\pi\alpha \frac{(q^2 - M_Z^2)}{\Lambda^2} \left[\frac{c_l}{s_l} f_{DW} - \frac{s_l}{c_l} f_{DB} \right] \quad (25)$$

Appendix B: General form of $\gamma\gamma \rightarrow \gamma\gamma$, γZ cross sections.

The possibility to use polarized or unpolarized $\gamma\gamma$ collisions in an LC operated in the $\gamma\gamma$ mode, through laser backscattering [16, 19] is described in [22, 4]. The assumption of Parity invariance leads to the following form for the $\gamma\gamma \rightarrow \gamma\gamma$, γZ cross section (note that a factor $\frac{1}{2}$ should be applied in the $\gamma\gamma \rightarrow \gamma\gamma$ case)

$$\begin{aligned} \frac{d\sigma}{d\tau d\cos\vartheta^*} = & \frac{d\bar{L}_{\gamma\gamma}}{d\tau} \left\{ \frac{d\bar{\sigma}_0}{d\cos\vartheta^*} + \langle \xi_2 \xi_2' \rangle \frac{d\bar{\sigma}_{22}}{d\cos\vartheta^*} + [\langle \xi_3 \rangle \cos 2\phi \frac{d\bar{\sigma}_3}{d\cos\vartheta^*} + \langle \xi_3' \rangle \cos 2\phi' \frac{d\bar{\sigma}'_3}{d\cos\vartheta^*}] \right. \\ & + \langle \xi_3 \xi_3' \rangle \left[\frac{d\bar{\sigma}_{33}}{d\cos\vartheta^*} \cos 2(\phi + \phi') + \frac{d\bar{\sigma}'_{33}}{d\cos\vartheta^*} \cos 2(\phi - \phi') \right] \\ & \left. + [\langle \xi_2 \xi_3' \rangle \sin 2\phi' \frac{d\bar{\sigma}_{23}}{d\cos\vartheta^*} - \langle \xi_3 \xi_2' \rangle \sin 2\phi \frac{d\bar{\sigma}'_{23}}{d\cos\vartheta^*}] \right\}, \end{aligned} \quad (26)$$

where

$$\frac{d\bar{\sigma}_0}{d\cos\vartheta^*} = \left(\frac{\beta_Z}{64\pi\hat{s}} \right) \sum_{\lambda_3\lambda_4} [|F_{++\lambda_3\lambda_4}|^2 + |F_{+-\lambda_3\lambda_4}|^2], \quad (27)$$

$$\frac{d\bar{\sigma}_{22}}{d\cos\vartheta^*} = \left(\frac{\beta_Z}{64\pi\hat{s}} \right) \sum_{\lambda_3\lambda_4} [|F_{++\lambda_3\lambda_4}|^2 - |F_{+-\lambda_3\lambda_4}|^2], \quad (28)$$

$$\frac{d\bar{\sigma}_3}{d\cos\vartheta^*} = \left(\frac{-\beta_Z}{32\pi\hat{s}} \right) \sum_{\lambda_3\lambda_4} \text{Re}[F_{++\lambda_3\lambda_4} F_{-+\lambda_3\lambda_4}^*], \quad (29)$$

$$\frac{d\bar{\sigma}'_3}{d\cos\vartheta^*} = \left(\frac{-\beta_Z}{32\pi\hat{s}} \right) \sum_{\lambda_3\lambda_4} \text{Re}[F_{++\lambda_3\lambda_4} F_{+-\lambda_3\lambda_4}^*], \quad (30)$$

$$\frac{d\bar{\sigma}_{33}}{d\cos\vartheta^*} = \left(\frac{\beta_Z}{64\pi\hat{s}} \right) \sum_{\lambda_3\lambda_4} \text{Re}[F_{+-\lambda_3\lambda_4} F_{-+\lambda_3\lambda_4}^*], \quad (31)$$

$$\frac{d\bar{\sigma}'_{33}}{d\cos\vartheta^*} = \left(\frac{\beta_Z}{64\pi\hat{s}} \right) \sum_{\lambda_3\lambda_4} \text{Re}[F_{++\lambda_3\lambda_4} F_{--\lambda_3\lambda_4}^*], \quad (32)$$

$$\frac{d\bar{\sigma}_{23}}{d\cos\vartheta^*} = \left(\frac{\beta_Z}{64\pi\hat{s}} \right) \sum_{\lambda_3\lambda_4} \text{Im}[F_{++\lambda_3\lambda_4} F_{+-\lambda_3\lambda_4}^*], \quad (33)$$

$$\frac{d\bar{\sigma}'_{23}}{d\cos\vartheta^*} = \left(\frac{\beta_Z}{64\pi\hat{s}} \right) \sum_{\lambda_3\lambda_4} \text{Im}[F_{++\lambda_3\lambda_4} F_{-+\lambda_3\lambda_4}^*], \quad (34)$$

are expressed in terms of the $\gamma\gamma \rightarrow \gamma\gamma$, γZ amplitudes given in Appendix A of [4], [5]. $\beta_Z = 1 - \frac{M_Z^2}{\hat{s}}$ and ϑ^* is the scattering angle in the $\gamma\gamma$ rest frame; $\tau \equiv s_{\gamma\gamma}/s_{ee}$. Note that only $d\bar{\sigma}_0/d\cos\vartheta^*$ is positive definite and that $\frac{d\bar{\sigma}'_3}{d\cos\vartheta^*}(\cos\vartheta^*) = \frac{d\bar{\sigma}_3}{d\cos\vartheta^*}(-\cos\vartheta^*)$, and $\frac{d\bar{\sigma}'_{23}}{d\cos\vartheta^*}(\cos\vartheta^*) = \frac{d\bar{\sigma}_{23}}{d\cos\vartheta^*}(-\cos\vartheta^*)$, which are identical in the case of the $\gamma\gamma$ final state.

A quick estimate of the unpolarized cross section can be done using the helicity amplitudes $F_{\lambda_1\lambda_2\lambda_3\lambda_4}$ mentioned in the text, eq.(5-7).

For a complete description one needs to take into account subleading amplitudes [4, 5]. $\frac{d\bar{L}_{\gamma\gamma}}{d\tau}$ is the $\gamma\gamma$ flux, and $\langle \xi_i \rangle \langle \xi_i \xi'_j \rangle$ are average stokes vectors describing the polarization state of the backscattered photon (possibly linearly polarized along the direction defined by the angle ϕ or ϕ' , see [4, 5]). These are computable simple functions of $\tau \equiv s_{\gamma\gamma}/s_{ee}$ and of the polarization degrees of the e^\pm and laser beams, given in ref.[19, 4].

References

- [1] M. Beccaria, P. Ciafaloni, D. Comelli, F. Renard, C. Verzegnassi, hep-ph/9906319.
- [2] "SUSY Virtual Effects at LEP2 Boundary", M. Beccaria, P. Ciafaloni, D. Comelli, F. Renard, C. Verzegnassi, E.P.J.C. to appear; see also J. Layssac, F.M. Renard and C. Verzegnassi, Phys. Lett.**B418**,134(1998).
- [3] "Light by Light Scattering at High Energy: a Tool to Reveal New Particles", G.J. Gounaris, P.I. Porfyriadis, F.M. Renard, hep-ph/9812378, Phys.Lett.**B452**(1999)76.
- [4] "The gamma gamma to gamma gamma process in the Standard and SUSY models at high energies", G.J. Gounaris, P.I. Porfyriadis, F.M. Renard, hep-ph/9902230, Eur.Phys.J.C, to appear.
- [5] "The $\gamma\gamma \rightarrow \gamma Z$ process and the search for virtual SUSY effects at high energies", G.J. Gounaris, J. Layssac, P.I. Porfyriadis, F.M. Renard, hep-ph/9904450, Eur.Phys.J.C, to appear.
- [6] F.M. Renard and C. Verzegnassi, Phys. Rev. D **52**, 1369 (1995); F.M. Renard and C. Verzegnassi, Phys. Rev. D **53**, 1290 (1996).
- [7] M. Beccaria, G. Montagna, F. Piccinini, F.M. Renard, C. Verzegnassi, Phys.Rev. **D58**,093014(1998).
- [8] G. Montagna, O. Nicrosini, G. Passarino, F. Piccinini, Comput.Phys.Commun. 93 1996.
- [9] H.P. Nilles, Phys.Rep. **110**,1(1984); H.E. Haber and G.L. Kane, Phys. Rep. **117**,75(1985); R. Barbieri, Riv.Nuov.Cim. **11**,1(1988); R. Arnowitt, A, Chamseddine and P. Nath, "Applied N=1 Supergravity (World Scientific, 1984); for a recent review see e.g. S.P. Martin, hep-ph/9709356.
- [10] K.Hagiwara, S.Ishihara, R.Szalapski, D.Zeppenfeld, Phys. Lett. **B283** (1992) 353 and Phys. Rev. **D48** (1993) 2182
- [11] Physics at LEP2, Proceedings of the Workshop-Geneva, Switzerland (1996), CERN 96-01, G. Altarelli, T. Sjostrand and F. Zwirner eds.
- [12] A. Blondel, F.M. Renard, L. Trentadue and C. Verzegnassi, Phys. Rev. D **54**, 5567 (1996).

- [13] K. Hagiwara, S. Matsumoto, and R. Szalapski, Phys. Lett. **B357** (1995) 411
- [14] M. Beccaria, F.M. Renard, S. Spagnolo and C. Verzegnassi, hep-ph/9810323, Phys.Lett.**B448**(1999)129.
- [15] F.M. Renard and C. Verzegnassi, Phys. Rev. **D55** (1997) 4370.
- [16] Opportunities and Requirements for Experimentation at a Very High Energy e^+e^- Collider, SLAC-329(1928); Proc. Workshops on Japan Linear Collider, KEK Reports, 90-2, 91-10 and 92-16; P.M. Zerwas, DESY 93-112, Aug. 1993; Proc. of the Workshop on e^+e^- Collisions at 500 GeV: The Physics Potential, DESY 92-123A,B,(1992), C(1993), D(1994), E(1997) ed. P. Zerwas; E. Accomando *et.al.* Phys. Rep. **C299** (1998) 299.
- [17] R.S. Chivucula, F.M. Renard, and C. Verzegnassi, Phys. Rev. **D57**(1998)2760.
- [18] G. Jikia and A. Tkabladze, Phys. Lett. **B332** (1994) 441; G. Jikia and A. Tkabladze, Phys. Lett. **B323** (1994) 453; E.W.N. Glover and J.J. van der Bij Nucl. Phys. **B313** (1989) 237;M.-z. Yang and X.j. Zhou Phys. Rev. **D52** (1995) 5018.
- [19] I.F. Ginzburg, G.L. Kotkin, V.G. Serbo and V.I. Telnov, Nucl. Instr. and Meth. **205**, (1983) 47; I.F. Ginzburg, G.L. Kotkin, V.G. Serbo, S.L. Panfil and V.I. Telnov, Nucl. Instr. and Meth. **219**,(1984) 5; J.H. Kühn, E.Mirkes and J. Steegborn, Z. f. Phys. **C57** (1993) 615.
- [20] R. Casalbuoni et al., hep-ph/9809523.
- [21] M. Chanowitz and M.K. Gaillard, Nucl. Phys. **B261** (1985) 379.
- [22] G.J. Gounaris and G. Tsirigoti, Phys. Rev. **D56** (1997) 3030, Erratum-ibid **D58** (1998) 059901.
- [23] S.Y. Choi et al, hep-ph/9806279, Eur.Phys.Jour.**C7**(1999)123.

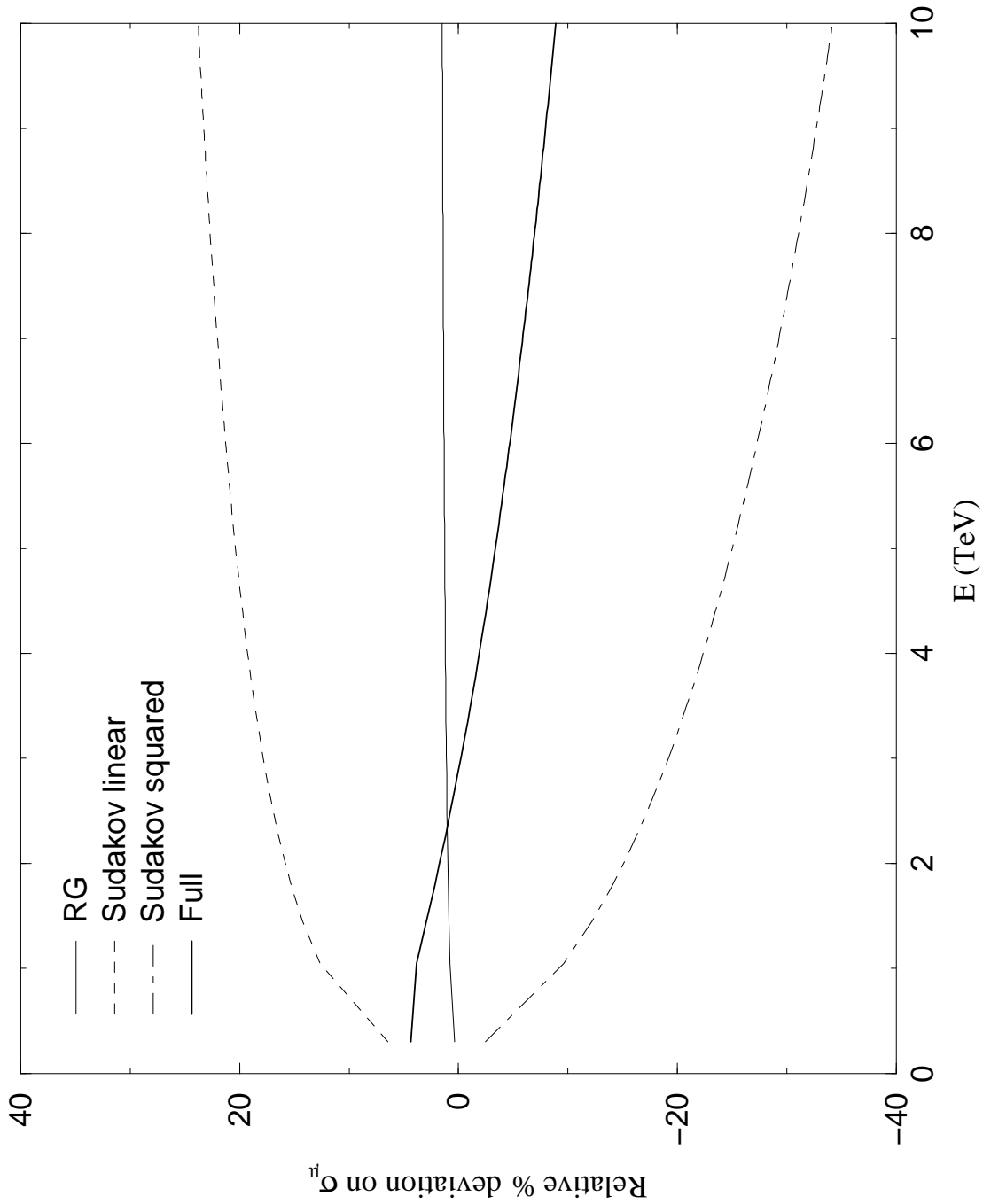


Figure 1: Logarithmic 1-loop Standard Model contributions to the asymptotic cross section $\sigma(e^+e^- \rightarrow \mu^+\mu^-)$.

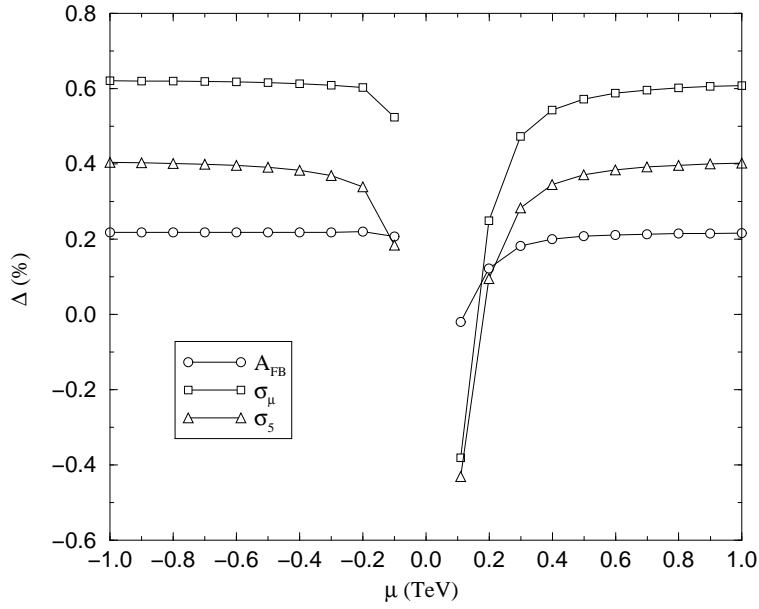


Figure 2: SUSY effects on the three considered observables with the mass of the lightest chargino fixed at 105 GeV and $\tan\beta = 1.6$. $m_{\tilde{q}}$ is fixed at 200 GeV and $m_{\tilde{l}}$ at 120 GeV.

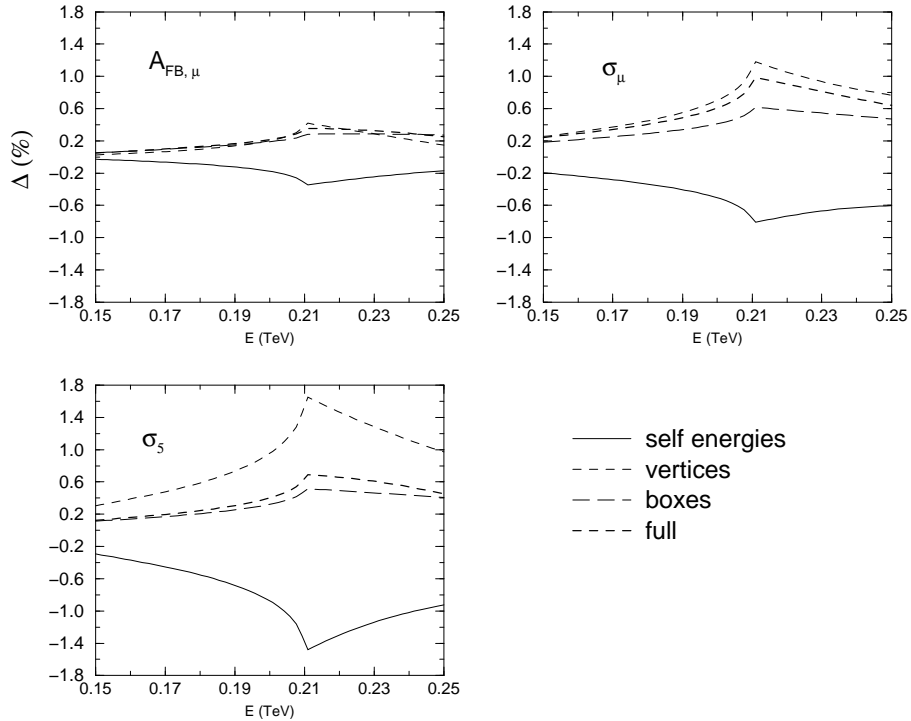


Figure 3: Selfenergy, box and vertex SUSY effects in the heavy sfermions-light chargino scenario (same parameters as in Fig.1 with a high μ value).

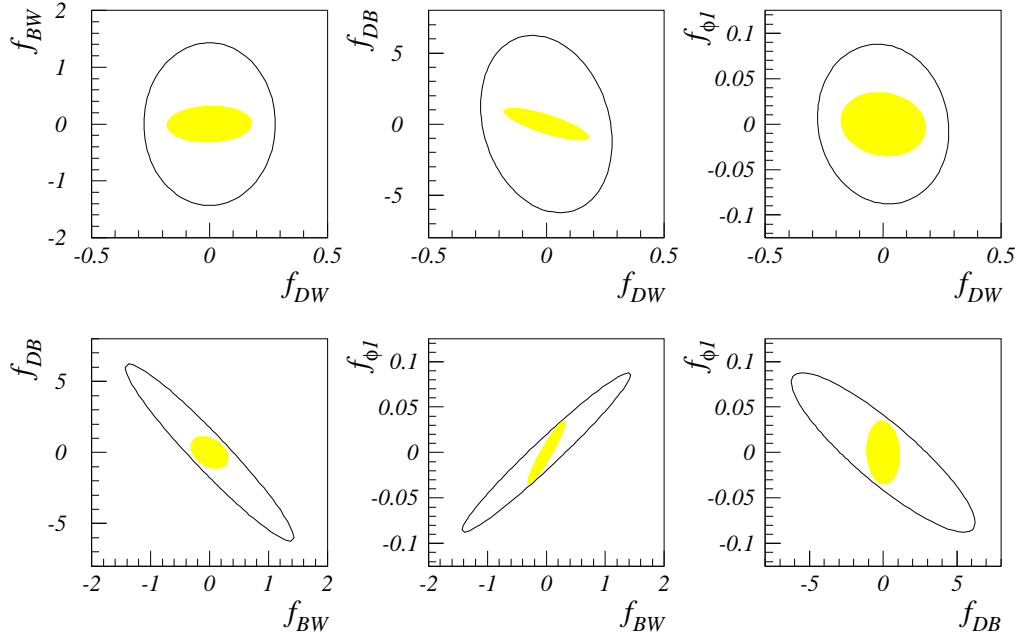
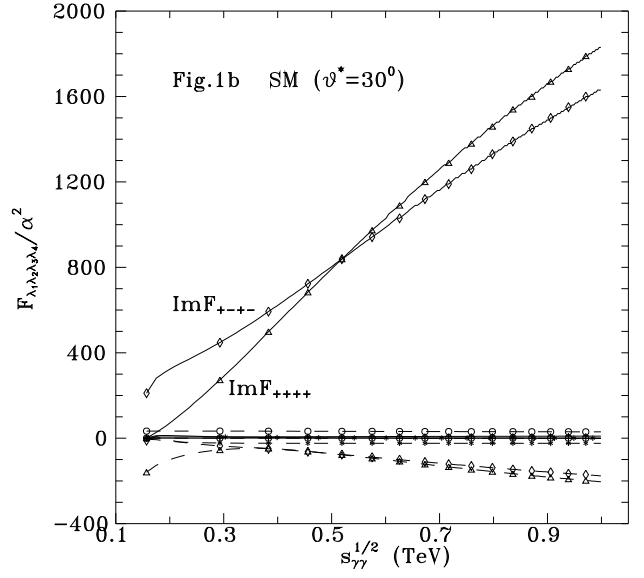
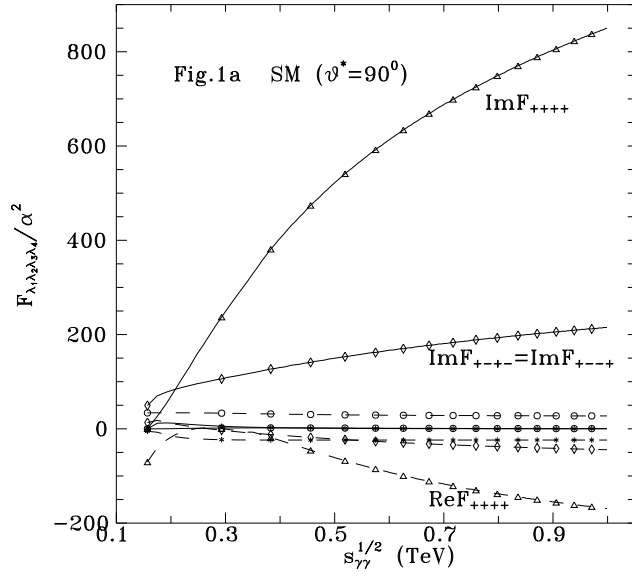
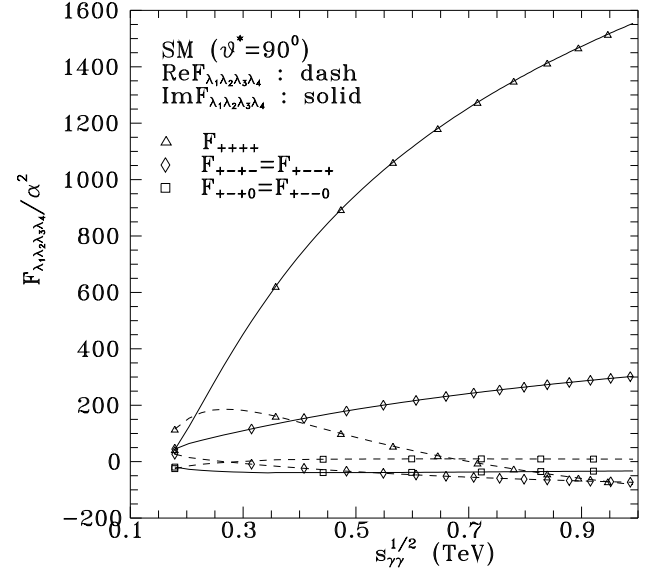
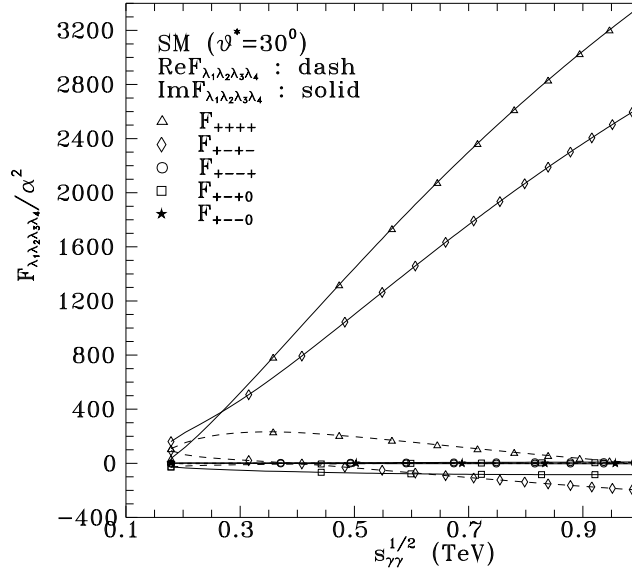


Figure 4: Projection of the $\chi^2 < \chi^2_{min} + 1$ region in the space of the four anomalous gauge couplings onto the six possible coordinate planes. The outer ellipses are obtained from low energy data only; the inner ones, by including the LEP2 data.



$\gamma\gamma \rightarrow \gamma\gamma$



$\gamma\gamma \rightarrow \gamma Z$

Figure 5: Imaginary (solid line) and real (dashed line) parts of the SM $\gamma\gamma \rightarrow \gamma\gamma$ and $\gamma\gamma \rightarrow \gamma Z$ helicity amplitudes at $\vartheta = 90^\circ$ and $\vartheta = 30^\circ$.

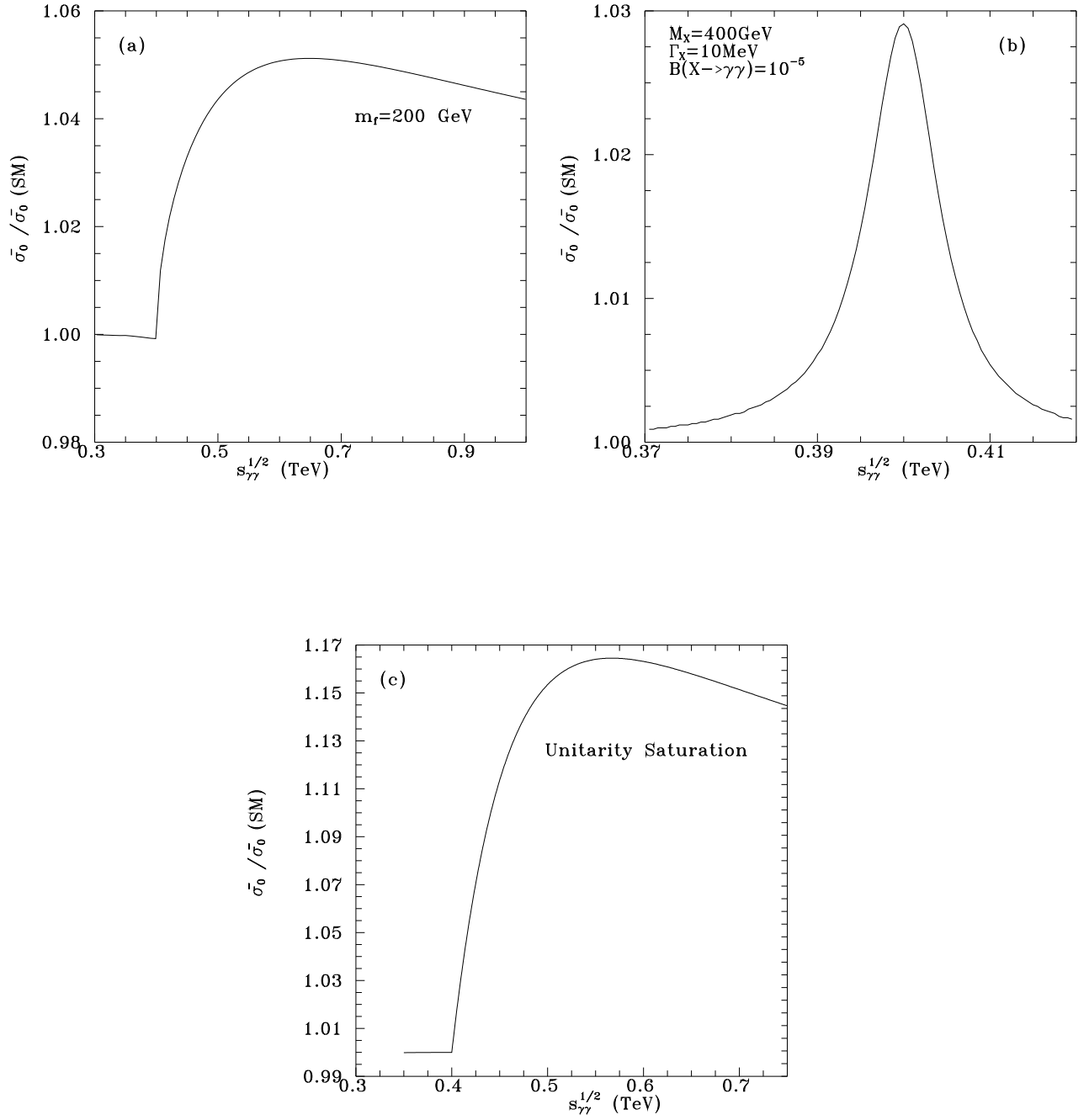


Figure 6: Relative magnitude with respect to the SM results, of the unpolarized $\gamma\gamma \rightarrow \gamma\gamma$ cross sections for a charge +1 fermion (a), a typical s-channel neutral resonance (b), and unitarity saturating amplitudes (c). In all cases the cross sections have been integrated in the c.m. angular range $30^\circ < \vartheta^* < 150^\circ$.

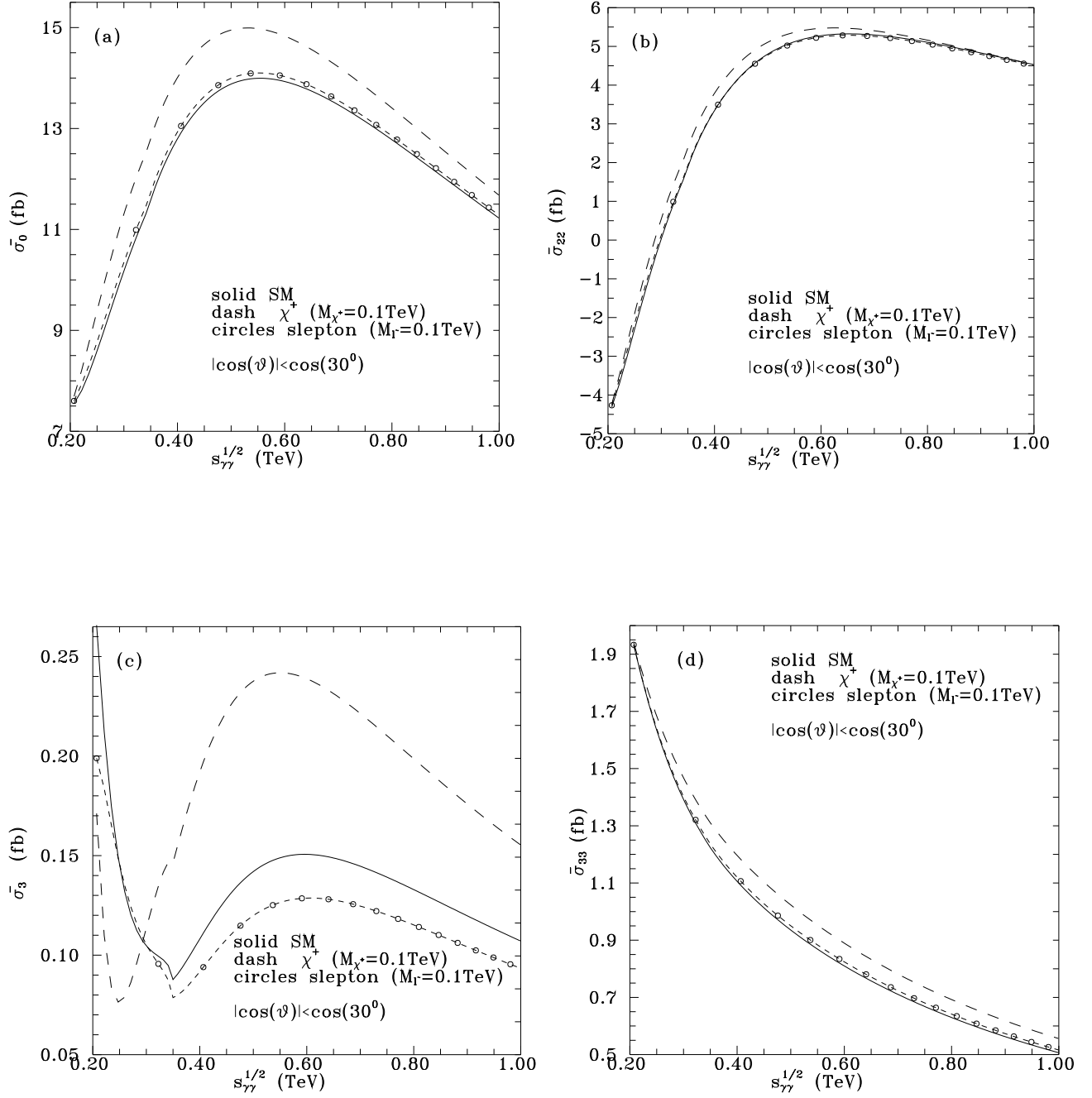


Figure 7: $\bar{\sigma}_0$, $\bar{\sigma}_{22}$, $\bar{\sigma}_3$, $\bar{\sigma}_{33}$ cross sections in $\gamma\gamma \rightarrow \gamma\gamma$ integrated over $|\cos(\vartheta^*)| < \cos(30^\circ)$. The SM and SUSY contributions induced by one chargino or one charged slepton with mass of 100 GeV, are also indicated.

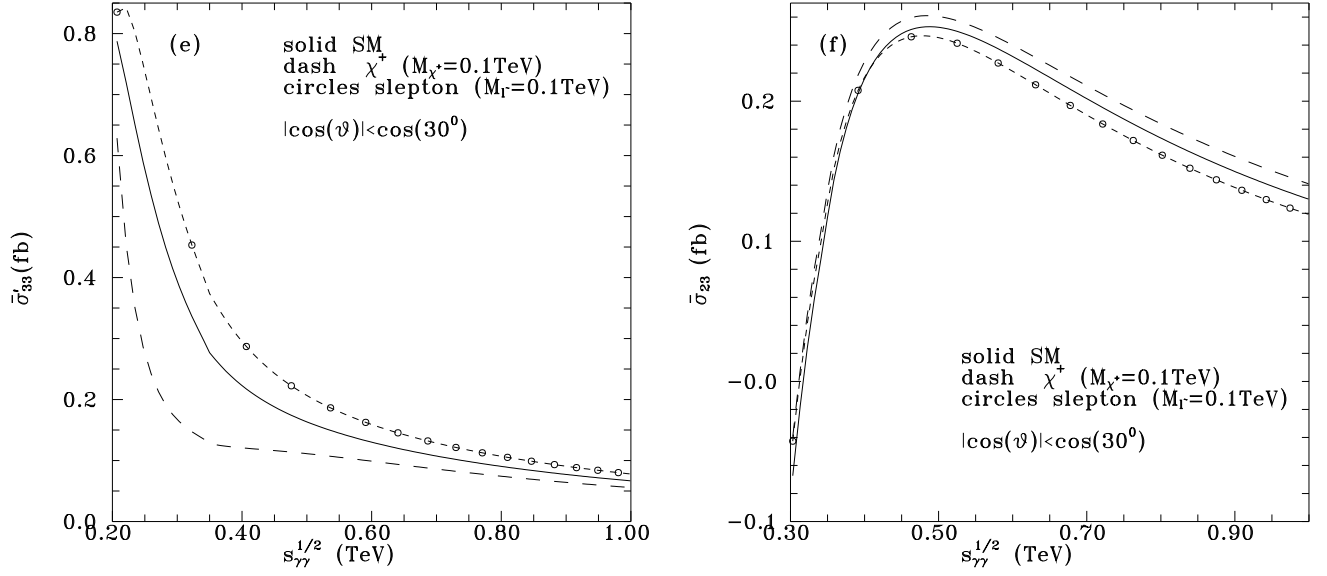


Figure 8: $\bar{\sigma}'_{33}$ and $\bar{\sigma}_{23}$ cross sections in $\gamma\gamma \rightarrow \gamma\gamma$ integrated over $|\cos(\vartheta^*)| < \cos(30^\circ)$. The SM and SUSY contributions induced by one chargino or one charged slepton with mass of 100 GeV, are also indicated.

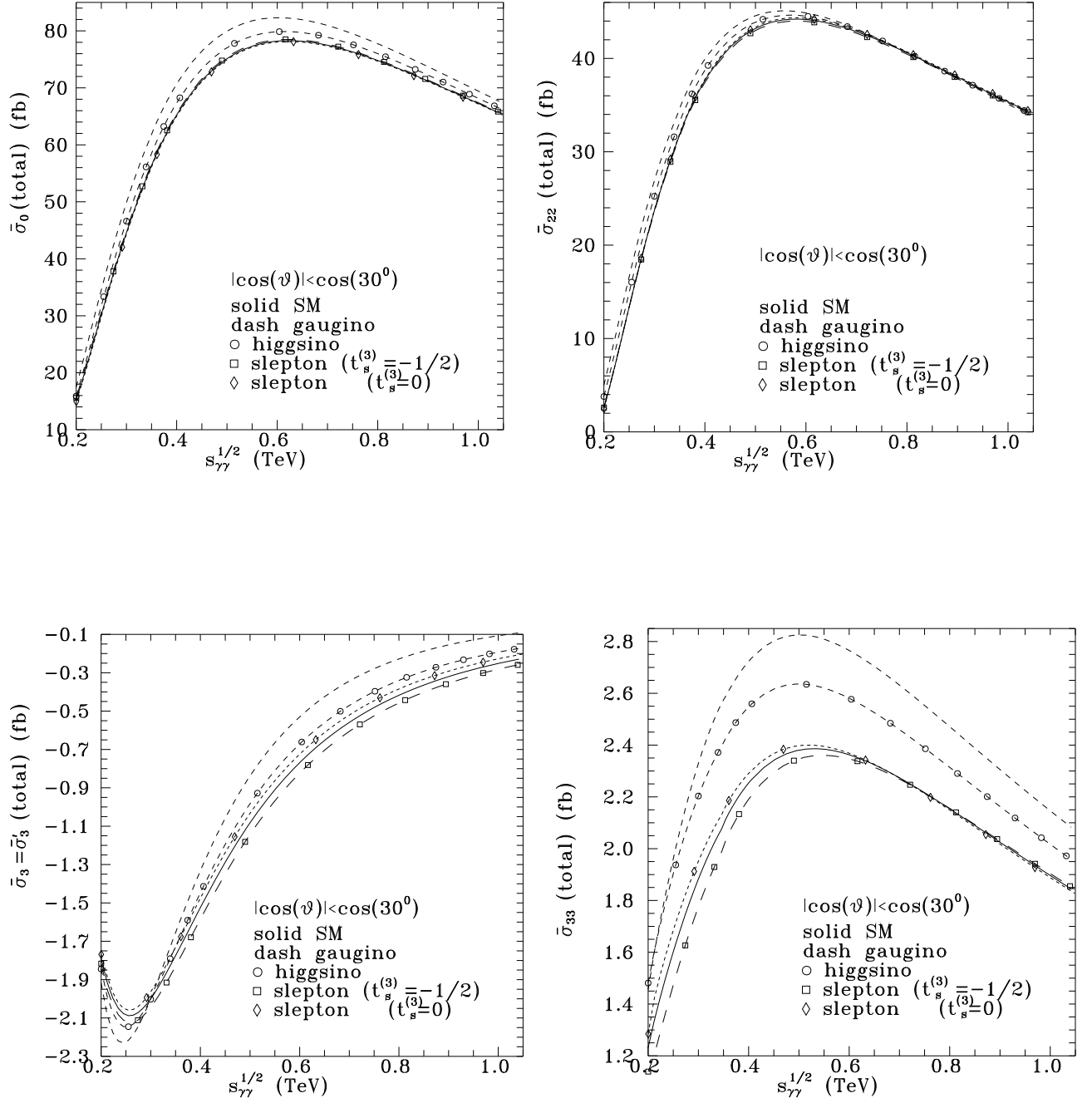


Figure 9: $\bar{\sigma}_0$, $\bar{\sigma}_{22}$, $\bar{\sigma}_3$, $\bar{\sigma}_{33}$ cross sections in $\gamma\gamma \rightarrow \gamma Z$ integrated over $|\cos(\vartheta^*)| < \cos(30^\circ)$. The SM and SUSY contributions induced by one chargino or one charged slepton with mass of 100 GeV, are also indicated.

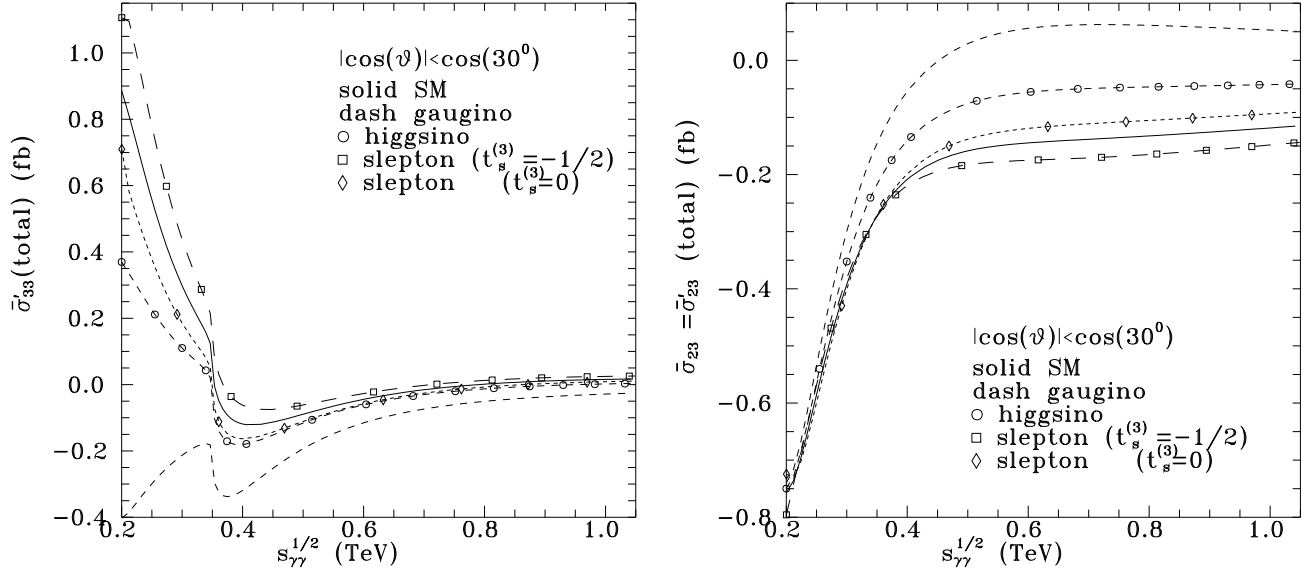


Figure 10: $\bar{\sigma}'_{33}$ and $\bar{\sigma}_{23}$ cross sections in $\gamma\gamma \rightarrow \gamma Z$ integrated over $|\cos(\vartheta^*)| < \cos(30^\circ)$. The SM and SUSY contributions induced by one chargino or one charged slepton with mass of 100 GeV, are also indicated.